Modelling the effects of bacterial cell state and spatial location on tuberculosis treatment: Insights from a hybrid multiscale cellular automaton model

Ruth Bowness[1,*], Mark Chaplain[2], Gibin Powathil[3], Stephen Gillespie[1]

[1] *School of Medicine, University of St Andrews, North Haugh, St Andrews, KY16 9TF, UK*
[2] *School of Mathematics and Statistics, University of St Andrews, North Haugh, St Andrews, KY16 9SS*
[3] *Department of Mathematics, Talbot Building, Swansea University, Singleton Park, Swansea, SA2 8PP*

Abstract

If improvements are to be made in tuberculosis (TB) treatment, an increased understanding of disease in the lung is needed. Studies have shown that bacteria in a less metabolically active state, which is associated with the presence of lipid bodies, are less susceptible to antibiotics, and recent results have highlighted the disparity in concentration of different compounds into lesions. Treatment success therefore depends critically on the responses of the individual bacteria that constitute the infection.

We propose a hybrid, individual-based approach that analyses spatio-temporal dynamics at the level of cells, linking individual cell behaviour with the macroscopic behaviour of cell organisation and the microenvironment. The individual cells (bacteria, macrophages and T cells) are modelled using a cellular automaton (CA) approach and we have incorporated the evolution of oxygen and chemokine dynamics within this hybrid model in order to study the effects of the microenvironment in TB therapies. We allow bacteria to switch states depending on oxygen concentration, which affects how they respond to treatment. Using this multiscale model, we investigate the role of bacterial cell state and of initial bacterial location on treatment outcome. We demonstrate that when bacteria are located further away from blood vessel sources, and when the immune response is unable to contain the less metabolically active bacteria near the start of the simulations, a less favourable outcome is likely.

Keywords:
Tuberculosis, Cellular automaton, Hybrid multiscale model, Chemotherapy, Bacteria

1. Introduction

Although tuberculosis (TB) has long been both preventable and curable, a person dies from tuberculosis every twenty seconds. Current treatment requires at least six months of multiple antibiotics to ensure complete cure and more effective drugs are urgently needed to shorten treatment. Recent clinical trials have not resulted in a shortening of therapy and there is a need to understand why these trials were unsuccessful and which new regimen should be chosen for testing in the costly long-term pivotal trial stage.

The current drug development pathway in tuberculosis is incompletely integrated and there are important unanswered questions at every stage. It remains unclear to what extent many preclinical methods capture the correct pharmacodynamic properties of a drug or reproduce the conditions under which it must act in the diseased host. *In vitro* methods may not accurately reflect the spectrum of physiological conditions found in natural populations of *M. tuberculosis* while *in vivo* systems may not exhibit sufficiently human-like pathology.

When *Mycobacterium tuberculosis* bacteria enter the lungs, a complex immune response ensues and results in the formation of granuloma structures. When these granulomas are unable to contain the bacteria, active disease develops. In patients with established disease, the outcome is perhaps determined by the ability of antibiotics to penetrate to the site of the infection: the granuloma. Granulomas have a central focus of debris, described as "caseous" which is characteristic of tuberculosis. These lesions continue to develop through a number of stages to form cavities, which are surrounded by fibrosis. All of these developments speak to the challenge of ensuring sufficient concentrations of antibiotic reach the site of infection.

It is increasingly recognised that *M.tb* is able to enter into a state in which it is metabolically less active and consequently much less susceptible to current antibiotics. This state, associated with the presence of lipid bodies in the mycobacterial cell can increase resistance by 15 fold (Hammond et al., 2015). Hence, it is very important to study and analyse the heterogeneity of the bacterial cell state and their spatial location so more effective treatment protocols can be developed.

Cellular automaton modelling (and individual-based modelling in general) has been used to model other diseases, most notably tumour development and progression in cancer (Powathil et al., 2012). The granuloma has been simulated previously through an agent-based model called 'GranSim' (Segovia-Juarez et al., 2004; Marino et al., 2011; Cilfone et al., 2013), which aims to reconstruct the immunological processes involved in the development of a granuloma. Recent iterations of the model have also started to address pharmacokinetic components (Pienaar et al., 2015). In this paper, we report the development of a hybrid-cellular automaton model to investigate the

role of bacterial cell state heterogeneity and bacterial position within the tuberculosis lesion on the outcome of disease.

2. The hybrid multiscale mathematical model

We consider a two dimensional computational grid (the spatial domain), where each grid point represents either a TB bacterium, a macrophage, a T cell, caseum, the cross-section of a blood vessel or the extracellular matrix which goes to make up the local microenvironment. The spatial size of this computational grid has been chosen in such a way that each automaton element is approximately the same size as the largest cell in the system. We note that a cellular automaton model is not the ideal framework to address the effects of interstitial pressure (real cells deform, while our individual cellular automaton elements do not, and accounting for this would require some form of viscoelastic tissue model or continuum model cf. Frieboes et al. (2009); Ribba et al. (2009)). For this reason we attempt to incorporate the effect of pressure through certain assumptions related to the transport properties and delivery rates of the oxygen and the chemotherapy drugs.

To simulate the spatio-temporal growth and evolution of the TB bacteria and their response to chemotherapeutic drugs, we assign four main components to each automaton element in the computational domain. These are: (1) cells - the automaton element is occupied either by a TB bacterium, a macrophage, a T cell, caseum or it is empty. If the automaton (grid) cell is occupied, automaton rules control the evolution; (2) the local oxygen concentration, whose evolution is modelled by a system of partial differential equation; (3) chemokine concentrations, modelled by a system of partial differential equations; (4) chemotherapeutic drug concentrations, modelled by a system of partial differential equations and (5) randomly distributed blood vessels from where the oxygen and chemotherapy are supplied within the domain. A schematic overview of the model is given in Figure 1.

2.1. The blood vessel network

At the tissue scale, we have incorporated the effects of a changing microenvironment by introducing oxygen dynamics to the model. This is achieved by incorporating a distribution of blood vessels (vasculature) in the model. Computationally, there are several ways of introducing vascular dynamics into the model depending on various temporal and spatial scales of interest (Anderson and Chaplain, 1998; Chaplain and Anderson, 2004). In our model, we have considered blood vessel cross sections distributed randomly throughout the two dimensional domain of the simulation with density $\phi_d = N_v/N^2$, where N_v is the number of vessel cross sections (Figure 2). This is reasonable if we assume that the blood vessels are perpendicular to the cross section of interest and there are no branching points through the plane of interest (Patel et al., 2001; Daşu et al., 2003). For computational convenience, we have ignored any temporal dynamics of these vessels, assuming the growth of TB cells is faster than that of the vessels within the time frame of our interest. This network of vessel cross sections is then used as a source of oxygen and drug distribution within the model. A detailed mathematical and computational description of these macroscopic dynamics are given in the following sections.

2.2. Oxygen dynamics

The macroscopic dynamics of oxygen concentration are modelled using a suitable partial differential equation incorporating vessels as sources, forming a continuous distribution within the simulation domain. If $O(\mathbf{x}, t)$ denotes the oxygen concentration at position $\mathbf{x}$ at time t, then its rate of change can be expressed as

$$\frac{\partial O(\mathbf{x},t)}{\partial t} = \nabla.(D_O(\mathbf{x})\nabla O(\mathbf{x},t)) + r_O m(\mathbf{x}) - \phi_O O(\mathbf{x},t)\text{cell}(\mathbf{x},t), \tag{1}$$

where $D_O(\mathbf{x})$ is the diffusion coefficient and ϕ_O is the rate of oxygen consumption by a cell at position x at time t ($\text{cell}(\mathbf{x}, t) = 1$ if position x is occupied by a TB bacterium at time t and zero otherwise). Here, $m(\mathbf{x})$ denotes the vessel cross section at position $\mathbf{x}$ ($m(\mathbf{x}) = 1$ for the presence of blood vessel at position $\mathbf{x}$, and zero otherwise); thus the term $r_O m(\mathbf{x})$ describes the production of oxygen at rate r_O. We assume that the oxygen is supplied through the pre-existing blood vessels, and then diffuses throughout the tissue feeding the cells within its diffusion limit. We do not consider any spatial changes in our vascular system. Since it has been observed that when a vessel is surrounded by a mass of caseum its perfusion and diffusion capabilities are seriously impaired, we have incorporated this in our model by considering a lower diffusion rate and a lower supply rate in the granuloma as compared to the normal vessels (Datta et al., 2015), i.e.

$$D_O = \begin{cases} \dfrac{D_O}{1.5} & \text{inside a granuloma} \\ D_O & \text{elsewhere in the domain,} \end{cases} \tag{2}$$

and

$$r_O = \begin{cases} \dfrac{r_O}{1.5} & \text{inside a granuloma} \\ r_O & \text{elsewhere in the domain.} \end{cases} \tag{3}$$

The formulation of the model is then completed by prescribing no-flux boundary conditions and an initial condition (Powathil et al., 2012). Figure 3 shows a representative profile of the spatial distribution of oxygen concentration after solving the Equation 1 with relevant parameters as discussed in the section, Section 2.5.

2.3. Chemotherapy treatments

In the present model we assume a maximum drug effect, allowing us to concentrate on the focus of this paper: the comparison of cell state and bacterial spatial location on treatment outcome. In future papers, the administration of drugs will more closely model the current reality. In this first iteration

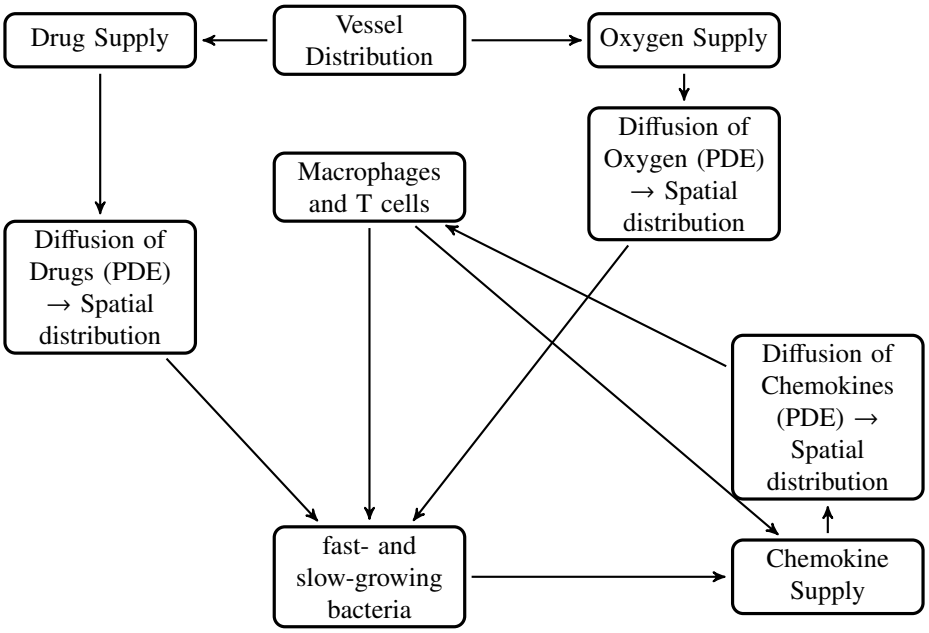

Figure 1: Schematic describing the basic processes in the CA

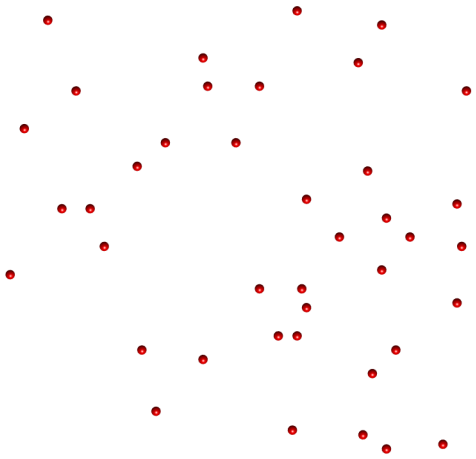

Figure 2: Plot illustrating one outcome of a random distribution of blood vessel cross sections throughout the spatial domain used in the cellular automaton simulations.

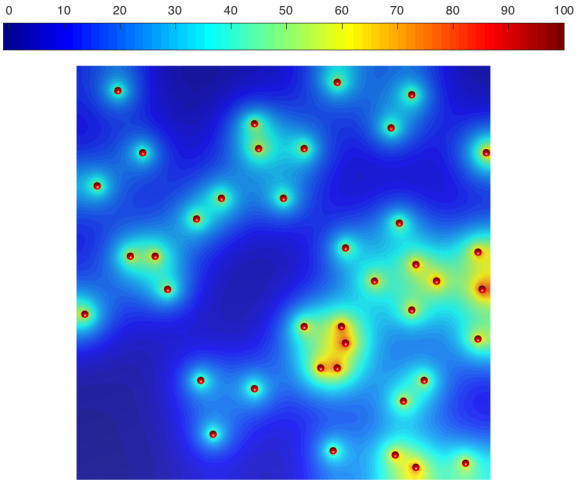

Figure 3: Plot showing the concentration profile of oxygen supplied from the vasculature. The red coloured spheres represent the blood vessel cross sections as shown in Figure 1 and the colour map shows the percentages of oxygen concentration.

of the model, the distribution of chemotherapeutic drug type i, $Drug_i(\mathbf{x},t)$ is governed by a similar equation as that of oxygen distribution (1), given by

$$\frac{\partial Drug_i(\mathbf{x},t)}{\partial t} = \nabla.(D_{Drugi}(\mathbf{x})\nabla Drug_i(\mathbf{x},t)) + r_{Drugi}m(\mathbf{x}) - \phi_{Drugi}Drug_i(\mathbf{x},t)\text{cell}(\mathbf{x},t) - \eta_{Drugi}Drug_i(\mathbf{x},t), \quad (4)$$

where $D_{Drugi}(\mathbf{x})$ is the diffusion coefficient of the drug, ϕ_{Drugi} is the rate by which the drug is taken in by a cell (assumed to be zero as it is negligible when compared to oxygen uptake), r_{Drugi} is the drug supply rate by the pre-existing vascular network and η_{Drugi} is the drug decay rate. Inside a granuloma structure, the diffusion and supply rate are lower to account for caseum impairing blood vessels and the fact that we know that diffusion into granulomata is lower than in normal lung tissue. Moreover, as the cells inside the granuloma are more densely packed than the normal tissue, the motility of drug molecules (hence, the diffusion) is more restricted within the granuloma than else-

where. Hence, similar to our assumptions for oxygen, these effects of pressure are taken into account through the following assumptions related to the transport properties and delivery rate of the drug:

$$D_{Drugi} = \begin{cases} \dfrac{D_{Drugi}}{1.5} & \text{inside the granuolma} \\ D_{Drugi} & \text{elsewhere in the domain,} \end{cases} \quad (5)$$

and

$$r_{Drugi} = \begin{cases} \dfrac{r_{Drugi}}{1.5} & \text{inside the granuloma} \\ r_{Drugi} & \text{elsewhere in the domain.} \end{cases} \quad (6)$$

To study the efficacy of the drug in killing bacteria, we have assumed a threshold drug concentration value, below which the drug has no effect on the bacteria. If the drug reaches a cell when it's concentration is above this level (which is different for fast- and slow-growing extracellular bacteria and for intracellular bacteria), then the bacterium will be killed and an empty space will be created (this will be described further in section 3.1).

2.4. Chemokines

Various molecules are released by macrophages and other immune cells, these molecules act as chemoattractants, attracting other cells to the site of infection. Although different chemokines perform different roles at various times, for this model, we can chosen to represent the multiple chemokines involved in the immune response as an aggregate chemokine value. Sources of chemokine are derived from infected, chronically infected and activated macrophages (Algood et al., 2003). The distribution of the chemokine molecules, $Ch(\mathbf{x}, t)$ is also governed in a similar way to the oxygen:

$$\frac{\partial Ch(\mathbf{x}, t)}{\partial t} = \nabla.(D_{Ch}(\mathbf{x})\nabla Ch(\mathbf{x}, t)) + r_{Ch}\text{cell}(\mathbf{x}, t) - \eta_{Ch}Ch(\mathbf{x}, t), \quad (7)$$

where $D_{Ch}(\mathbf{x})$ is the diffusion coefficient of the chemokines, r_{Ch} is the chemokine supply rate by the macrophages at position $\mathbf{x}$ at time t ($\text{cell}(\mathbf{x}, t) = 1$ if position $\mathbf{x}$ is occupied by an infected, chronically infected or activated macrophage at time t and zero otherwise) and η_{Ch} is the chemokine decay rate.

2.5. Parameter estimation

To simulate this model and to make biologically relevant deductions, it is important to use accurate parameters values within the model. Most of the parameters are chosen from previous mathematical and experimental papers (see Table 1 and Table 2 for a summary of the parameter values).

We take hours as the time scale for the cellular automaton model. We have assumed a cell length of 20 μm, which is the approximate size of the biggest cell in our system, the macrophage (Krombach et al., 1997). The simulations are carried out within a two dimensional domain with a grid size $N = 100$, which can simulate an area of lung tissue 2 $mm \times 2$ mm. The space step was set to $\Delta x = \Delta y = 0.2$ and the time step in the simulation was set to be $\Delta t = 0.001$, with one time step corresponding to 3.6 s. This was calculated by considering the fastest process in our system, the diffusion of oxygen.

The oxygen dynamics are governed by a reaction diffusion equation, where the parameters are mainly chosen from the literature (Macklin et al., 2012). The oxygen diffusion length scale L is often considered to be approximately equal to 100 μm and the value of the diffusion constant is taken as 2×10^{-5} cm^2/s (Owen et al., 2004). Using these and the relation $L = \sqrt{D/\phi}$, the mean oxygen uptake can be approximately estimated as 0.2 s^{-1}. The oxygen supply through the blood vessel is approximately taken as 8.2×10^{-3} mols s^{-1} (Matzavinos et al., 2009). The appropriate nondimensionalisation will yield a time scale of T=0.001 hr and hence each time step is set to be 0.001 hr for both CA time step as well as for the oxygen dynamics. The length scale of 100 μm will give a square grid of length $\Delta x \times L$=20 μm, approximate diameter of a cell. The parameters that are used in the equations governing the dynamics of chemotherapy and chemokines are also chosen in a similar fashion. Oxygen is lighter in comparison to the drugs with a molecular weight of 32 amu (Hlatky and Alpen, 1985) and hence it diffuses faster than most of the drugs and the chemokines, which are much heavier. The chemokine molecules diffuse at the slowest rate, being heavier than most drugs. One of the drugs under the current study, rifampicin has a molecular weight of 822.9 amu (PubChem Compound Database). To obtain or approximate its diffusion coefficient, its molecular mass was compared against the molecular masses of known compounds and consequently taken to be 1.7×10^{-6} cm^{2}s^{-1}. A similar analysis is done with isoniazid, pyrazinamide and ethambutol, and the parameter values are given in Table 1. The decay rate of these drugs are calculated using the half life values of the drugs obtained from the literature and are also given in Table 1. The threshold drug concentrations, $DrugKill_f$, $DrugKill_s$ and $DrugKill_{Mi}$, below which the drug has no effect on the TB cells have chosen to be the average density of total drugs delivered through the vessels (total drug delivered/ total number of grid points) and the total drug given is kept same for all drugs types. A relative threshold is chosen here in order to compare the effects of cell state and location of bacteria, rather than studying any optimisation protocols for drug dosage. Values of 10^{-6} cm^{2}s^{-1} to 10^{-7} cm^{2}s^{-1} have been reported as diffusion constants for chemokine molecules (Francis and Palsson, 1997). The half-life for IL-8, an important chemokine involved in the immune response of *M. tuberculoisis*, has been shown to be 2-4 hours (Walz et al., 1996). We use a diffusion rate of 10^{-6} cm^{2}s^{-1} and a half-life of 2 hours in our simulations.

Other model parameters will be discussed in the next section and are summarised in Table 2.

Table 1: Diffusion and decay parameters

Drug/Chemokine	Diffusion rate (cm^2s^{-1})	Decay rate (hr^{-1})
Rifampicin	1.7×10^{-6}	0.17
Isoniazid	1.5×10^{-5}	0.35
Pyrazinamide	1.6×10^{-5}	0.12
Ethambutol	1.3×10^{-5}	0.2
Chemokine	10^{-6}	0.347

3. Cellular automaton rules

The entire multiscale model is simulated over a prescribed time duration, currently set to 672 hours (4 weeks), and a vector containing all cell positions is updated at every time step. The oxygen dynamics, chemokine dynamics and chemotherapy dynamics are simulated using finite difference schemes.

3.1. Rules for the extracellular bacteria

The CA begins with two clusters of bacteria on the grid; one cluster of fast-growing bacteria and one cluster of slow-growing bacteria. These initial bacteria replicate following a set of rules and produce a cluster of cells on a regular square lattice with no-flux boundary conditions. The fast- and slow-growing bacteria are assigned a replication rate; Rep_f for the fast-growing and Rep_s for the slow-growing. When a bacterium is marked for replication, its neighbourhood of order 3 is checked for an empty space. The neighbourhood type alternates between a Moore neighbourhood and a Von Neumann neighbourhood to avoid square/diamond shaped clusters, respectively. If a space in the neighbourhood exists, a new bacterium is placed randomly in one of the available grid cells. If there are no spaces in the neighbourhood of order 3, the cell is marked as 'resting'. This process mimics quoram sensing. At each time step, the neighbourhood of these 'resting' cells is re-checked so that they can start to replicate again as soon as space becomes available.

As this multiscale model evolves over time, the cells are simulated in an orderly fashion using the CA model, and these cells further influence the spatial distribution of oxygen since they consume oxygen for their essential metabolic activities. As the bacteria proliferate, the oxygen demand increases creating an inbalance between the supply and demand which will eventually create a state where the cells are deprived of oxygen. Bacteria can change between fast- growing and slow-growing states, depending on the oxygen concentration, scaled from 0 to 100, at their location. Fast-growing bacteria where the oxygen concentration is below O_{low} will become slow-growing, and slow-growing bacteria can turn to fast-growing in areas where the oxygen concentration is above O_{high}.

3.2. Rules for the macrophages

There are 4 types of macrophage in our system: resting (Mr), active (Ma), infected (Mi) and chronically infected (Mci). There are Mr_{init} resting macrophages randomly placed on the grid at the start of the simulation. These resting macrophages can become active when the chemokine moelcules in their location is above $Chem_{ra}$, where the chemokine concentration is scaled similarly to the oxygen from 0 to 100. Active Macrophages will kill fast-growing extracellular bacteria with a probability Ma_{fkill} and slow-growing extracellular bacteria with probability Ma_{skill}. If the resting macrophages encounter bacteria, they become infected and can become chronically infected when they phagocytose more than N_{ici} bacteria. Chronically infected macrophages can only contain N_{cib} intracellular bacteria, after which they burst. Bursting macrophages distribute bacteria randomly into their Moore neighbourhood of order 3 and the grid cell where the macrophage was located becomes caseum.

While the oxygen and chemotherapy enters the system via the blood vessel network, the chemokines are secreted by the infected, chronically infected and activated macrophages. Macrophages move in biased random walks, with probabilities calculated as a function of the chemokine concentration of its Moore neighbourhood. Resting, infected and chronically infected macrophages are randomly assigned a lifespan, M_{life} days, and active macrophages live for Ma_{life} days. Resting macrophages move every t_{moveMr} minutes, active macrophages move every t_{moveMa} hours and infected/chronically infected macrophages move every t_{moveMi} hours. Resting macrophages are recruited from the blood vessels with a probability of Mr_{recr} in response to the chemokine level at their location.

3.3. Rules for the T cells

The T cells enter the system once the extracellular bacterial load reaches T_{enter} and move in a biased random walk, similar to the macrophages. T cells are recruited from the blood vessels with a probability T_{recr}, in response to the chemokine level at those locations. They live for T_{life}, and move every t_{moveT} minutes. Activated T cells are immune effector cells that can kill chronically infected macrophages. If a T cell encounters an infected or chronically infected macrophage, it kills the macrophage (and all intracellular bacteria) with probability T_{kill} and that grid cell becomes caseum.

3.4. Rules for the Chemotherapy

Chemotherapy is administered at t_{drug} hours, a randomly chosen time between two values. This mimics the variability in time that patients seek medical attention for their disease. The drug can kill the bacteria when the concentration is over $DrugKill_f$ or $DrugKill_s$, for the fast- and slow-growing bacteria respectively. The chemotherapy can also kill intracellular bacteria, by killing infected/chronically infected macrophages if the concentration is over $DrugKill_{Mi}$.

4. Results

In order to study the relative importance of bacterial cell state and initial spatial location of bacteria, we study two scenarios: one with fixed blood vessel distribution and initial bacterial locations, and another where the vessel distribution and the initial locations of the extracellular bacteria are determined randomly for each simulation. We run four simulations for each scenario. Line plots showing bacterial numbers during these simulations are shown in Figure 4 for the fixed scenario and Figure 8 for

Table 2: Parameters. When there is a range for a value, it is set randomly by the model.

Parameter	Description	Value	Source
Rep_f (hours)	Replication rate of fast-growing bacteria	15-32	(Shorten et al., 2013)
Rep_s (hours)	Replication rate of slow-growing bacteria	48-96	(Hendon-Dunn et al., 2016)
O_{low}	O_2 threshold for fast→slow-growing bacteria	6	Estimated - see Section 4.1
O_{high}	O_2 threshold for slow→fast-growing bacteria	65	Estimated - see Section 4.1
Mr_{init}	Initial number of Mr in the domain	105	(Cilfone et al., 2013)
$Chem_{ra}$	Chemokine threshold for Mr→Ma	50	Estimated
Ma_{fkill}	Probability of Ma killing fast-growing bacteria	0.8	Estimated
Ma_{skill}	Probability of Ma killing slow-growing bacteria	0.7	Estimated
N_{ici}	Number of bacteria needed for Mi→Mci	10	(Cilfone et al., 2013)
N_{cib}	Number of bacteria needed for Mci to burst	20	(Cilfone et al., 2013)
M_{life} (days)	Lifespan of Mr, Mi and Mci	0-100	(Van Furth et al., 1973)
Ma_{life} (days)	Lifespan of Ma	10	(Segovia-Juarez et al., 2004)
t_{moveMr} (mins)	Time interval for Mr movement	20	(Segovia-Juarez et al., 2004)
t_{moveMa} (hours)	Time interval for Ma movement	7.8	(Segovia-Juarez et al., 2004)
t_{moveMi} (hours)	Time interval for Mi/Mci movement	24	(Segovia-Juarez et al., 2004)
Mr_{recr}	Probability of Mr recruitment	0.07	(Cilfone et al., 2013)
T_{enter}	Bacteria needed for T cells to enter the system	50	(Cilfone et al., 2013)
T_{recr}	Probability of T cell recruitment	0.02	(Cilfone et al., 2013)
T_{life} (days)	Lifespan of T cells	0-3	(Segovia-Juarez et al., 2004)
T_{kill}	Probability of T cell killing Mi/Mci	0.75	(Cilfone et al., 2013)
t_{moveT} (mins)	Time interval for T cell movement	10	(Segovia-Juarez et al., 2004)
t_{drug} (hours)	TIme at which drug is administered	168-336	Estimated
$DrugKill_f$	Drug needed to kill fast-growing bacteria	3	Estimated
$DrugKill_s$	Drug needed to kill slow-growing bacteria	15	(Hammond et al., 2015)
$DrugKill_{Mi}$	Drug needed to kill intracellular bacteria	9	Giancarlo, LSTM

the random distribution scenario. Plots showing the spatial distribution of all cells for four simulations are shown in Figure 5-7 for the fixed scenario and Figure 9-11 for the random distribution scenario. Three time frames are depicted: the start of the simulation (Figure 5 and Figure 9), just before the drug enters the domain (Figure 6 and Figure 10) and the end of the simulation (Figure 7 and Figure 11).

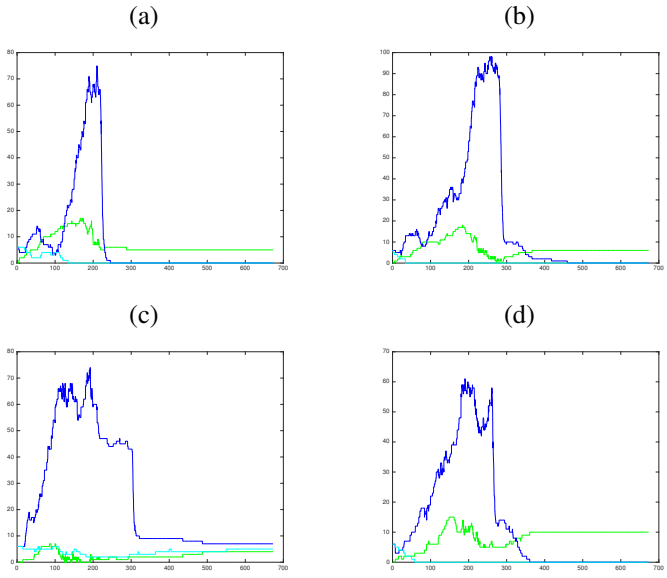

Figure 4: Plots showing bacterial numbers for four simulations, (a)-(d), with a fixed blood vessel distribution and initial extracellular bacterial positions. Fast-growing extracellular bacteria (dark blue), slow-growing extracellular bacteria (cyan) and intracellular bacteria (green).

For the fixed distribution scenario, the four simulations have differences but by the end of the simulations (at 4 weeks) the number of extracellular bacteria is either zero or very low. In all simulations we also see the immune cells killing or controlling the slow-growing bacteria and the majority of the fast-growing bacteria are killed by the chemotherapy. The simulations for the randomly assigned distributions show very different outcomes. In simulation (a), the extracellular bacteria are all killed by 36 hours with 2 intracellular bacteria persisting at 4 weeks. In simulation (b), the fast-growing extracellular bacteria build to over 80 until the chemotherapy kill them all. At the end of this simulation there are 3 slow-growing extracellular bacteria and 11 intracellular bacteria. Simulation (c) sees the immune response controlling all fast-growing cells by 82 hours, whereas the slow-growing bacteria continue to replicate, with over 60 by the end of the simulation. Simulation (d) ends with 26 fast-growing extracellular bacteria and 21 intracellular, where the slow-growing cells are controlled by the immune response by 30 hours.

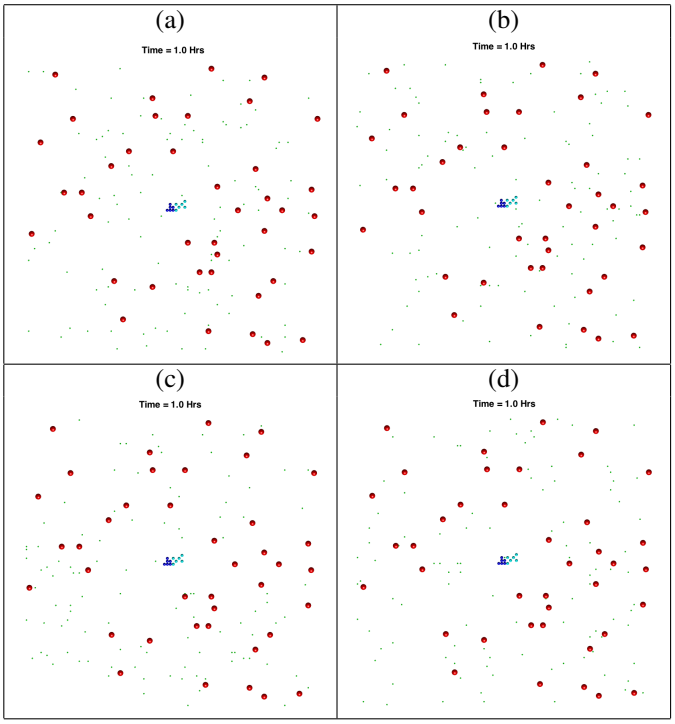

Figure 5: Plots showing the spatial distribution of all cells at the start of the four simulations (a)-(d), with fixed vessel distribution and initial bacterial location. Red circles depict the blood vessels, black circles depict the caseum, blue circles show the fast-growing extracellular bacteria, cyan circles show the slow-growing extracellular bacteria, green dots depict macrophages (with darker green for the infected/chronically infected macrophages) and yellow dots depict the T cells.

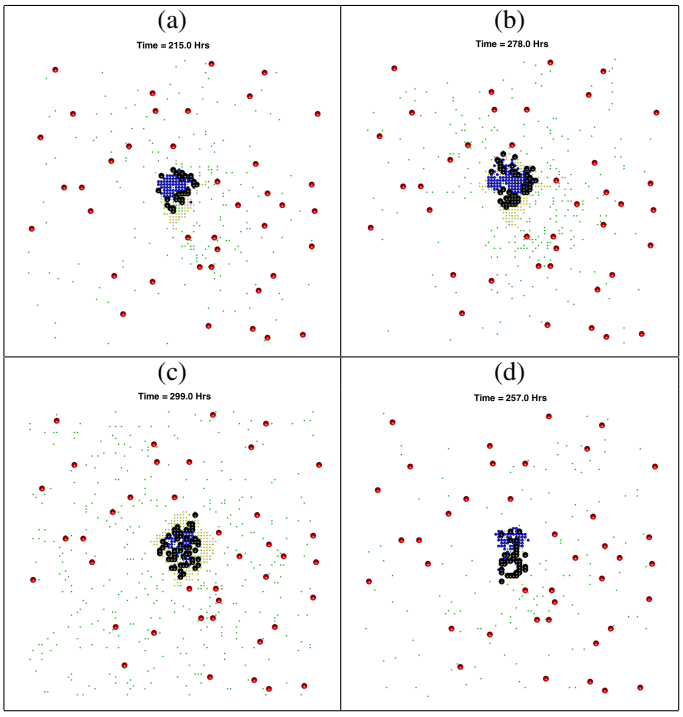

Figure 6: Plots showing the spatial distribution of all cells, just before the drug enters the domain, for the four simulations (a)-(d), with fixed vessel distribution and initial bacterial location. Red circles depict the blood vessels, black circles depict the caseum, blue circles show the fast-growing extracellular bacteria, cyan circles show the slow-growing extracellular bacteria, green dots depict macrophages (with darker green for the infected/chronically infected macrophages) and yellow dots depict the T cells.

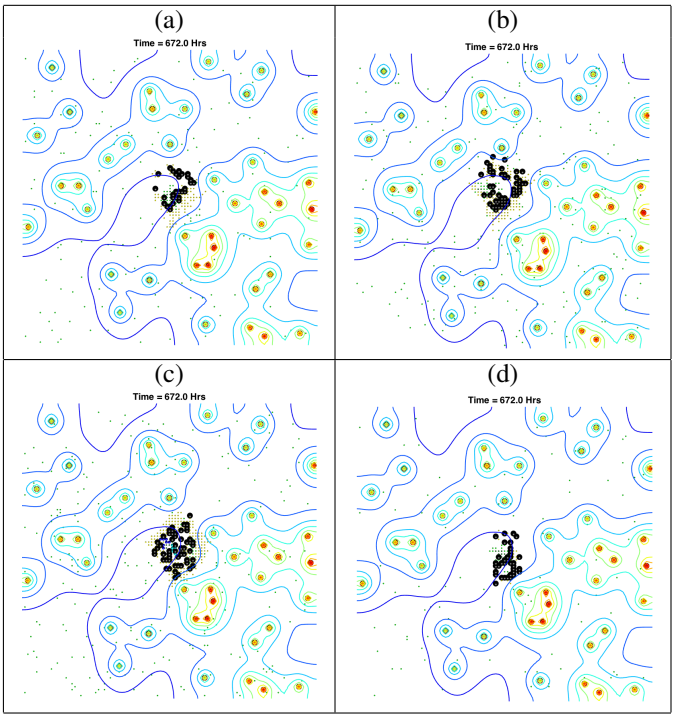

Figure 7: Plots showing the spatial distribution of all cells and contour lines of the chemotherapy at the end of the four simulations (a)-(d), with fixed vessel distribution and initial bacterial location. Red circles depict the blood vessels, black circles depict the caseum, blue circles show the fast-growing extracellular bacteria, cyan circles show the slow-growing extracellular bacteria, green dots depict macrophages (with darker green for the infected/chronically infected macrophages) and yellow dots depict the T cells.

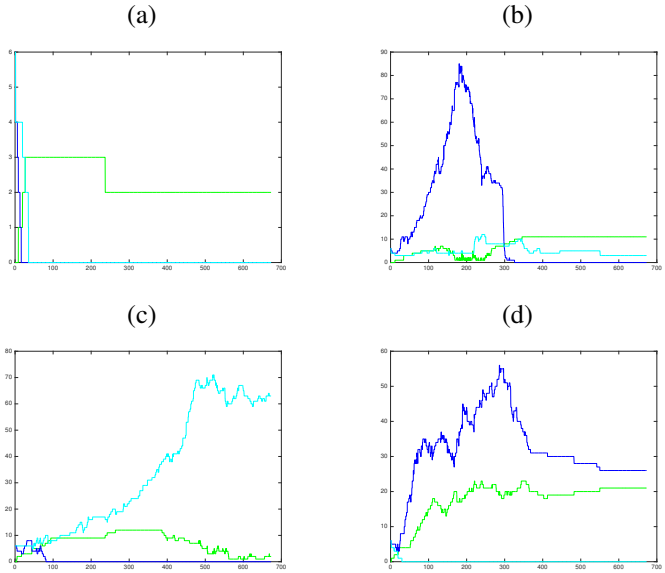

Figure 8: Plots showing bacterial numbers for four simulations, (a)-(d), with randomly selected blood vessel distribution and initial extracellular bacterial positions. Fast-growing extracellular bacteria (dark blue), slow-growing extracellular bacteria (cyan) and intracellular bacteria (green).

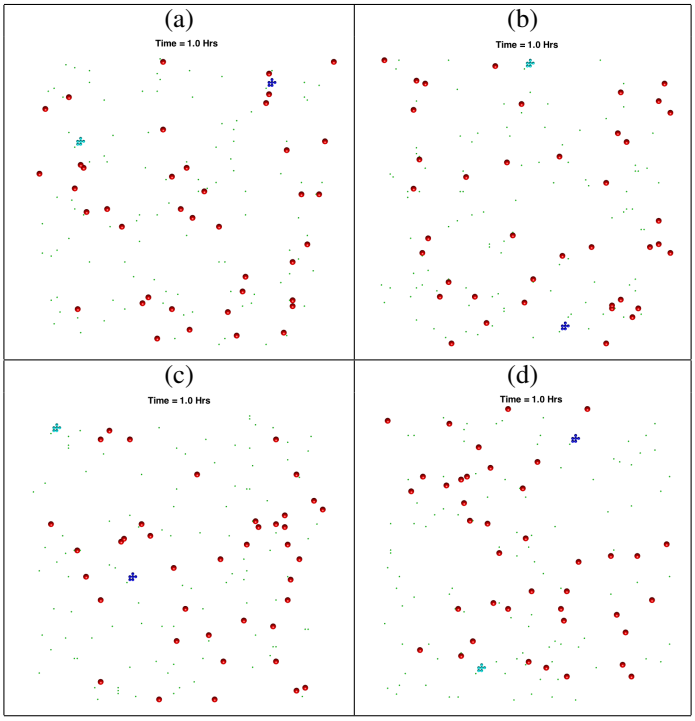

Figure 9: Plots showing the spatial distribution of all cells at the start of the four simulations (a)-(d), with randomly selected blood vessel distribution and initial extracellular bacterial positions. Red circles depict the blood vessels, black circles depict the caseum, blue circles show the fast-growing extracellular bacteria, cyan circles show the slow-growing extracellular bacteria, green dots depict macrophages (with darker green for the infected/chronically infected macrophages) and yellow dots depict the T cells.

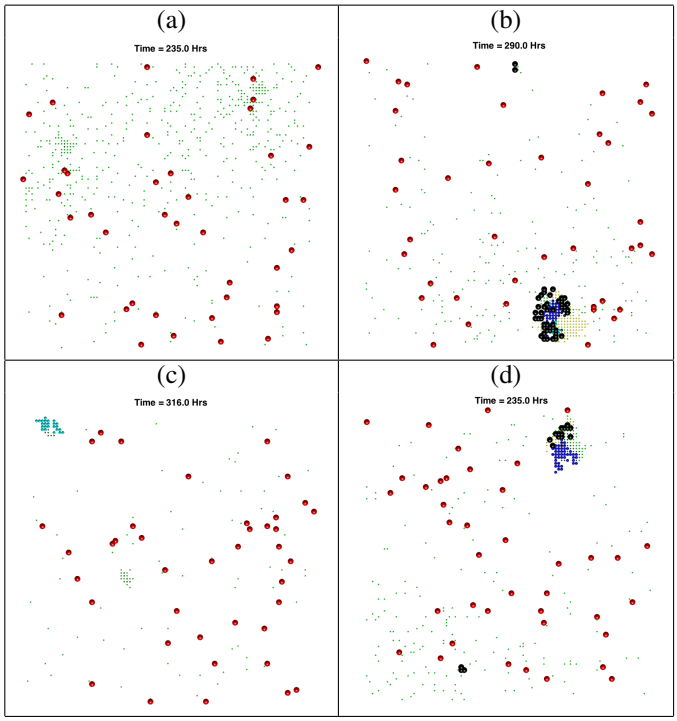

Figure 10: Plots showing the spatial distribution of all cells, just before the drug enters the domain, for the four simulations (a)-(d), with randomly selected blood vessel distribution and initial extracellular bacterial positions. Red circles depict the blood vessels, black circles depict the caseum, blue circles show the fast-growing extracellular bacteria, cyan circles show the slow-growing extracellular bacteria, green dots depict macrophages (with darker green for the infected/chronically infected macrophages) and yellow dots depict the T cells.

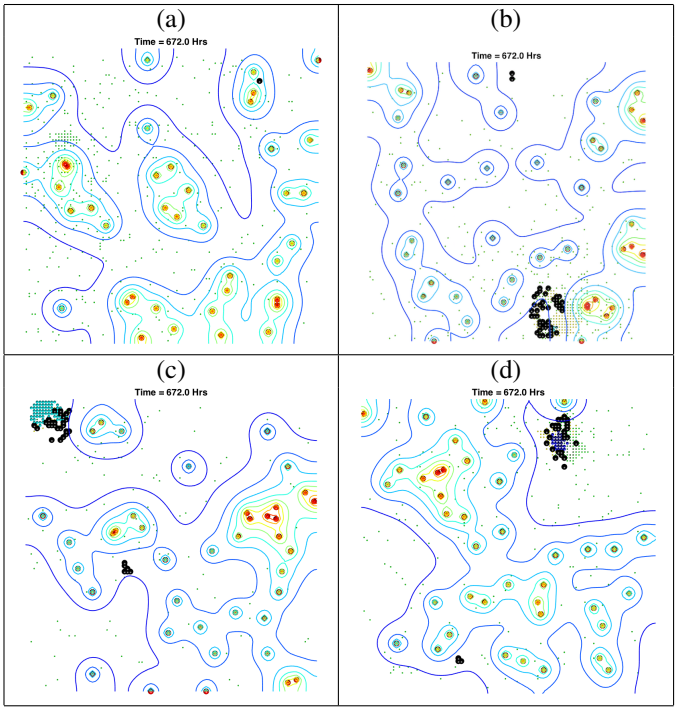

Figure 11: Plots showing the spatial distribution of all cells and contour lines of the chemotherapy at the end of the four simulations (a)-(d), with randomly selected blood vessel distribution and initial extracellular bacterial positions. Red circles depict the blood vessels, black circles depict the caseum, blue circles show the fast-growing extracellular bacteria, cyan circles show the slow-growing extracellular bacteria, green dots depict macrophages (with darker green for the infected/chronically infected macrophages) and yellow dots depict the T cells.

4.1. Oxygen thresholds for bacterial cell states

Although the above simulations were run with fixed parameter estimates, outlined in Table 2, we also ran some simulations with different values of O_{low} and O_{high} to see how this changed the results. Figure 12 shows three plots of the fast- and slow-growing cells (shown the the blue/cyan lines, respectively), with O_{high} fixed at 65 and O_{low} altered. These plots support the estimates chosen in Table 2, $O_{low} = 6$ and $O_{high} = 65$. Movies of these simulations are available online which confirm the conclusions made below. In (a) we see the effect of having a lower threshold for fast-growing cells to become slow-growing, with $O_{low} = 3$, in (b) $O_{low} = 6$, as per previous simulations and in (c), O_{low} has a higher threshold of 9. In simulation (a), the bacteria do not change state during the entire simulation, Figure 12 (a) supports this as we do not see an increase in the cyan line that corresponds with a drop in the blue. Simulation (b) has $O_{low} = 6$, as in previous simulations, and here we see some transfer from fast- to slow-growing during the 120 hours. For simulation (c), however, the fast-growing cells transfer to slow-growing almost immediately.

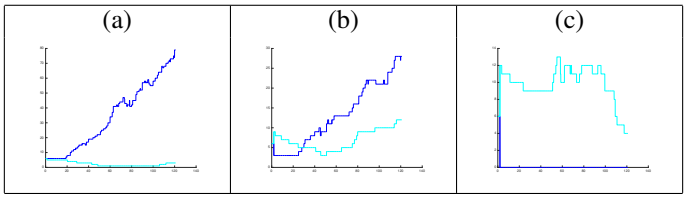

Figure 12: Plots of the fast- (blue) and slow-growing (cyan) extracellular bacteria for the first 120 hours.

Similarly, we ran three simulations where O_{low} is held at 6 and O_{high} is altered. Figure 13 shows plots of the fast- and slow-growing bacteria for these three simulations. In simulation (a), where $O_{high} = 55$, the slow-growing cells all change to fast-growing very near to the beginning of the simulation. Simulation (b) shows some slow-growing bacteria becoming fast-growing around 15 hours when O_{high} is set as in Table 2 at 65, and simulation (c) shows no transfer from fast- to slow-growing when $O_{high} = 75$.

These test simulations support us choosing $O_{low} = 6$ and $O_{high} = 65$.

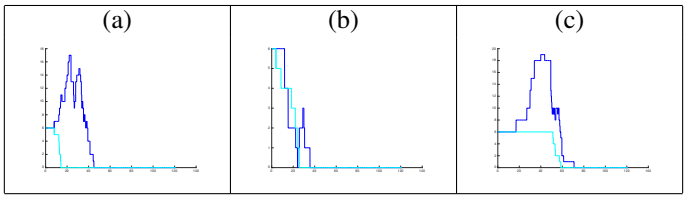

Figure 13: Plots of the fast- (blue) and slow-growing (cyan) extracellular bacteria for the first 120 hours.

5. Discussion

Individual-based models have already been shown to be useful in understanding tuberculosis disease progression (Segovia-Juarez et al., 2004; Marino et al., 2011; Cilfone et al., 2013). Here we have built a hybrid cellular automaton model that incorporates oxygen dynamics, which allows bacteria to change cell states. In addition to focusing on bacterial cell state, we also investigate changes in spatial location of the bacteria.

We show that position of bacteria in relation to the source of drugs alters the outcome of simulations. When bacteria are located far from the blood vessels, a poor outcome at the end of the simulation is more probable. This is in most part due to the poor diffusion of the drugs to these remote areas but also because the source of the immune cells is also the blood vessels and so there tends to be a weaker immune response before treatment begins. Another important feature of our model is that of caseation: when chronically infected macrophages burst or T cells kill infected macrophages, that grid cell becomes caseum. Hence, as macrophages move chemotactically towards the clusters of bacteria, a caseous granuloma starts to form and this caseum inhibits drug diffusion. In simulations where bacteria are surrounded by caseum, they often remain at the end of the simulation. This has implications for long-term outcome of patients.

We have also shown that bacterial cell state has an impact on simulations. Outcome tends to be worse in simulations where the immune response is unable to contain the LR bacteria, as these drugs are less susceptible to the antibiotics. Hence the spatial location of these bacteria in relation to the blood vessels is particularly important. There are relatively few publications that define the susceptibility of LR mycobacteria in relation to the standard or new anti-tuberculosis drugs.

In future iterations of the model we will explore the effect of fibrosis and cavity formation on outcome, building on recent concepts on lesional drug concentrations (Prideaux et al., 2015; Via et al., 2015).

We have shown that this type of spatial modelling approach is useful. Our preliminary simulations confirm the importance of bacterial cell state and also highlight the importance of spatial location of the bacteria. Perhaps it is thought obvious that spatial location of the bacteria is a key factor in treatment outcome but mathematical models to date have not highlighted this fact. Studies have focused on PK based on serum and simulations of ELF BL. Our modelling has shown that anatomical considerations may be important when chronic infection creates an anaerobic environment and fibrosis around cavities. Our simulations show that in cases when the caseum forms around the bacteria, a worse long-term outcome is more probable. This reflects what has long been known about the importance of caseum in defining outcome in TB. Treatment is compounded further by bacterial cell state, which increases functional MIC of bacteria that can be more difficult to kill due to poor penetration. Future models could address this with enhanced understanding of the effect of dormancy or phenotypic resistance. This indicates the importance of work to define lesional PK (Prideaux et al., 2015; Via et al., 2015).

6. References

Algood, H. M. S., Chan, J., Flynn, J. L., 2003. Chemokines and tuberculosis. Cytokine & growth factor reviews 14 (6), 467–477.

Anderson, A. R., Chaplain, M., 1998. Continuous and discrete mathematical models of tumor-induced angiogenesis. Bulletin of mathematical biology 60 (5), 857–899.

Chaplain, M., Anderson, A., 2004. Mathematical modelling of tumour-induced angiogenesis: network growth and structure. In: Angiogenesis in Brain Tumors. Springer, pp. 51–75.

Cilfone, N. A., Perry, C. R., Kirschner, D. E., Linderman, J. J., 2013. Multi-scale modeling predicts a balance of tumor necrosis factor-α and interleukin-10 controls the granuloma environment during mycobacterium tuberculosis infection. PloS one 8 (7), e68680.

Daşu, A., Toma-Daşu, I., Karlsson, M., 2003. Theoretical simulation of tumour oxygenation and results from acute and chronic hypoxia. Physics in medicine and biology 48 (17), 2829.

Datta, M., Via, L. E., Chen, W., Baish, J. W., Xu, L., Barry 3rd, C. E., Jain, R. K., 2015. Mathematical model of oxygen transport in tuberculosis granulomas. Annals of Biomedical Engineering, 1–10.

Francis, K., Palsson, B. O., 1997. Effective intercellular communication distances are determined by the relative time constants for cyto/chemokine secretion and diffusion. Proceedings of the National Academy of Sciences 94 (23), 12258–12262.

Frieboes, H. B., Edgerton, M. E., Fruehauf, J. P., Rose, F. R., Worrall, L. K., Gatenby, R. A., Ferrari, M., Cristini, V., 2009. Prediction of drug response in breast cancer using integrative experimental/computational modeling. Cancer research 69 (10), 4484–4492.

Hammond, R. J., Baron, V. O., Oravcova, K., Lipworth, S., Gillespie, S. H., 2015. Phenotypic resistance in mycobacteria: is it because i am old or fat that i resist you? Journal of Antimicrobial Chemotherapy 70 (10), 2823–2827.

Hendon-Dunn, C. L., Doris, K. S., Thomas, S. R., Allnutt, J. C., Marriott, A. A. N., Hatch, K. A., Watson, R. J., Bottley, G., Marsh, P. D., Taylor, S. C., et al., 2016. A flow cytometry method for rapidly assessing m. tuberculosis responses to antibiotics with different modes of action. Antimicrobial agents and chemotherapy, AAC–02712.

Hlatky, L., Alpen, E., 1985. Two-dimensional diffusion limited system for cell growth. Cell Proliferation 18 (6), 597–611.

Krombach, F., Münzing, S., Allmeling, A.-M., Gerlach, J. T., Behr, J., Dörger, M., 1997. Cell size of alveolar macrophages: an interspecies comparison. Environmental health perspectives 105 (Suppl 5), 1261.

Macklin, P., Edgerton, M. E., Thompson, A. M., Cristini, V., 2012. Patient-calibrated agent-based modelling of ductal carcinoma in situ (dcis): from microscopic measurements to macroscopic predictions of clinical progression. Journal of theoretical biology 301, 122–140.

Marino, S., El-Kebir, M., Kirschner, D., 2011. A hybrid multi-compartment model of granuloma formation and t cell priming in tuberculosis. Journal of theoretical biology 280 (1), 50–62.

Matzavinos, A., Kao, C.-Y., Green, J. E. F., Sutradhar, A., Miller, M., Friedman, A., 2009. Modeling oxygen transport in surgical tissue transfer. Proceedings of the National Academy of Sciences 106 (29), 12091–12096.

Owen, M. R., Byrne, H. M., Lewis, C. E., 2004. Mathematical modelling of the use of macrophages as vehicles for drug delivery to hypoxic tumour sites. Journal of theoretical biology 226 (4), 377–391.

Patel, A. A., Gawlinski, E. T., Lemieux, S. K., Gatenby, R. A., 2001. A cellular automaton model of early tumor growth and invasion: the effects of native tissue vascularity and increased anaerobic tumor metabolism. Journal of Theoretical Biology 213 (3), 315–331.

Pienaar, E., Cilfone, N. A., Lin, P. L., Dartois, V., Mattila, J. T., Butler, J. R., Flynn, J. L., Kirschner, D. E., Linderman, J. J., 2015. A computational tool integrating host immunity with antibiotic dynamics to study tuberculosis treatment. Journal of theoretical biology 367, 166–179.

Powathil, G. G., Gordon, K. E., Hill, L. A., Chaplain, M. A., Sep 2012. Modelling the effects of cell-cycle heterogeneity on the response of a solid tumour to chemotherapy: biological insights from a hybrid multiscale cellular automaton model. J. Theor. Biol. 308, 1–19.

Prideaux, B., Via, L. E., Zimmerman, M. D., Eum, S., Sarathy, J., O'Brien, P., Chen, C., Kaya, F., Weiner, D. M., Chen, P.-Y., et al., 2015. The association between sterilizing activity and drug distribution into tuberculosis lesions. Nature medicine 21 (10), 1223–1227.

Ribba, B., You, B., Tod, M., Girard, P., Tranchand, B., Trillet-Lenoir, V., Freyer, G., 2009. Chemotherapy may be delivered based on an integrated view of tumour dynamics. Systems Biology, IET 3 (3), 180–190.

Segovia-Juarez, J. L., Ganguli, S., Kirschner, D., Dec 2004. Identifying control mechanisms of granuloma formation during M. tuberculosis infection using an agent-based model. J. Theor. Biol. 231 (3), 357–376.

Shorten, R., McGregor, A., Platt, S., Jenkins, C., Lipman, M., Gillespie, S., Charalambous, B., McHugh, T., 2013. When is an outbreak not an outbreak? fit, divergent strains of mycobacterium tuberculosis display independent evolution of drug resistance in a large london outbreak. Journal of Antimicrobial Chemotherapy 68 (3), 543–549.

Van Furth, R., Diesselhoff-den Dulk, M. M., Mattie, H., 1973. Quantitative study on the production and kinetics of mononuclear phagocytes during an acute inflammatory reaction. The Journal of experimental medicine 138 (6), 1314–1330.

Via, L. E., Savic, R., Weiner, D. M., Zimmerman, M. D., Prideaux, B., Irwin, S. M., Lyon, E., O?Brien, P., Gopal, P., Eum, S., et al., 2015. Host-mediated bioactivation of pyrazinamide: Implications for efficacy, resistance, and therapeutic alternatives. ACS infectious diseases 1 (5), 203–214.

Walz, A., Kunkel, S., Strieter, R., Koch, A., Strieter, R., 1996. Chemokines in disease.